The emission characteristics of liquid-crystal lasers

S. M. Morris
A. D. Ford
C. Gillespie
M. N. Pivnenko
O. Hadeler
H. J. Coles

Abstract — Liquid-crystal lasers exhibit narrow linewidth, large coherence area, and low threshold laser emission. Moreover, the wavelength of the laser line can be readily tuned using a variety of different external stimuli, including electric fields. These combined features make them particularly attractive as compact tunable laser light sources. Recent experimental results with regards to the emission characteristics of chiral nematic photonic band-edge lasers are discussed. This type of liquid-crystal laser consists of a self-organizing one-dimensional photonic band structure and a gain medium in the form of a laser dye. Some of the generic features that are observed for these lasers are discussed, including the typical emission linewidth of the laser line, the change in emission energy of the laser for high excitation energies and high pump repetition rates, and the dependence of the excitation threshold and slope efficiency on the cell thickness. In addition, how the performance changes when either the molecular structure of the chiral nematic host or the gain medium is varied is considered. To conclude, results are presented on the laser emission for a wide-temperature-range blue phase I band-edge laser which consists of a self-organizing three-dimensional photonic band structure.

Keywords — *Photonic band-edge laser, dye, chiral nematic, blue phase.*

1 Introduction

Band-edge lasing in photonic crystals and liquid crystals has attracted widespread attention from the scientific community within recent years.[1–4] The reason for this is twofold. First, the phenomena of lasing at the edge of a photonic band gap (PBG) offers new challenges with respect to understanding the interaction of light as well as the emission characteristics in periodic dielectric structures. Second, due to the low-threshold large coherence area,[5] and tunability aspects this type of laser is of interest from a technological point of view. Potential applications include wide-area projection displays, telecommunications, devices for opto-medical applications, and lab-on-a-chip components.

The attraction of using liquid crystals for band-edge lasers is connected with the fact that the macroscopic properties can be manipulated using external stimuli. This in turn results in changes in the spectral position and bandwidth of the PBG. Consequently, numerous reports have demonstrated wavelength tuning in the form of UV illumination to provoke structural alterations through trans-cis conformation changes,[6–9] temperature changes so as to alter both the pitch and the optical properties,[10,11] mechanical stress applied to cholesteric elastomers,[12] and electric fields parallel and perpendicular to the helix axis.[13–15] In addition to the tuning capabilities, liquid crystals which contain a chiral component spontaneously organize to form photonic band structures with a periodic dielectric constant in one dimension (chiral nematic and chiral smectic phases[16,17]) or in three dimensions (blue phases I[18] and II[19]). Even though lasing has been demonstrated in all of these phases, most of the experimental and theoretical work has been concentrated on band-edge lasing from the chiral nematic phase.

In this paper, we present a review of our recent experimental work. We begin by considering the generic features that are observed for chiral nematic band-edge lasers such as the dependence on pump-spot size, pump repetition rate, and cell thickness. Following this, the changes in the emission properties that are observed for variations in the macroscopic properties of a chiral nematic host are discussed. We then go on to describe changes in the emission characteristics for several different commercially available laser dyes. In the final section, lasing from a wide-temperature-range blue phase I liquid crystal is demonstrated.

2 Sample preparations

Each laser sample was prepared by dissolving both a low concentration of chiral dopant and a laser dye into a nematic host. The actual components and compositions by weight are described in each section. The resulting mixtures were placed in a bake oven for a period of 24 hours so that a diffusive mixing process takes place. Samples were then capillary filled into a cell in the isotropic phase and subsequently cooled slowly to the required operating temperature. The laser cells are essentially the same as simple single-pixel displays with rubbed polyimide alignment layers plus indium tin oxide (ITO) electrodes on the glass substrates. Here, the pixels are 5×5 mm and the distance between electrodes is of the order of microns (see Sec. 3.4 below).

3 Generic features

For the following measurements, a dye-doped chiral nematic liquid-crystal sample was prepared. This consisted of a

The authors are with the Centre of Molecular Materials for Photonics and Electronics, Electrical Engineering Division, Cambridge University Engineering Department, 9 JJ Thomson Ave., Cambridge, CB3 0FA, U.K.; hjc37@cam.ac.uk.

nematogen host (E49, Merck NB-C), a high twisting power chiral dopant (BDH1281, Merck NB-C), and the laser dye 4-(dicyanomethylene)-2-methyl-6-(4-dimethylaminostryl) -4*H*-pyran (DCM, Lambda Physik). E49 is a well-known nematic liquid crystal that is a mixture of cyanobiphenyls, oxycyanobiphenyls, and cyanoterphenyls. It was chosen because it is liquid crystalline at room temperature and exhibits a broad nematic range up to 100°C. Consequently, at our operating temperature (T = 30°C), the nematic mesophase is well below the clearing point.

The concentration of chiral dopant required was determined by the following criteria. The gain maximum of DCM occurs at a wavelength of λ = 610 nm and is broad, ranging from 600 to 620 nm. Therefore, to achieve maximum efficiency, one band edge had to be matched to this gain maximum. The preferred band edge (either short-wavelength or long wavelength) was determined by whether the transition dipole moment of the dye aligns parallel or perpendicular to the director. For DCM in E49, the dye aligns preferentially parallel to the director, and thus the long-wavelength band edge was matched to the gain maximum of DCM. To achieve this, a concentration of 4.0 wt.% BDH1281 was required. The concentration of DCM was 2.0 wt.%. The sample, referred to herein as DCM-E49* (where the asterisk indicates chirality), was positioned at the focus of a Q-switched Nd:YAG laser and was optically pumped at λ = 532 nm with one pulse (5-nsec width) every second. The laser emission from the sample is collected in the forward direction over a narrow solid angle and the emission energies are then doubled to take into account the emission into the backward direction.[20] The details of the experiment are given elsewhere.[17]

3.1 Emission spectrum

The emission spectrum of the DCM-E49* laser at T = 30°C, for a cell thickness of d = 7.5 μm, is shown in Fig. 1. It can be seen that the laser line (secondary y-axis) occurs at 604.65 nm and the linewidth is Δλ ~ 0.10 nm. This emission spectrum was recorded using a 0.04-nm-resolution spectrometer (HR2000, Ocean Optics). Also shown is the transmission spectrum for white light which is plotted on the primary y-axis. The inset of the figure allows for a closer inspection of the laser line in comparison to the transmission maximum of the first peak on the long-wavelength side of the PBG. It is apparent that the laser line is centred at a slightly longer wavelength than the peak of the first transmission maximum on the long-wavelength side of the band edge. This offset is to be expected for finite thickness samples because the laser mode does not correspond exactly with the band edge. According to John and Quang,[20] the photon localization length, ξ_{loc}, can be expressed as $\xi_{loc} \sim c/\sqrt{\omega_{BE}|\omega_{BE}-\omega_a|}$, where ω_a is the frequency of the emitted photon and ω_{BE} is the frequency corresponding to the band edge. For the case shown in the figure, the localization length is found to be

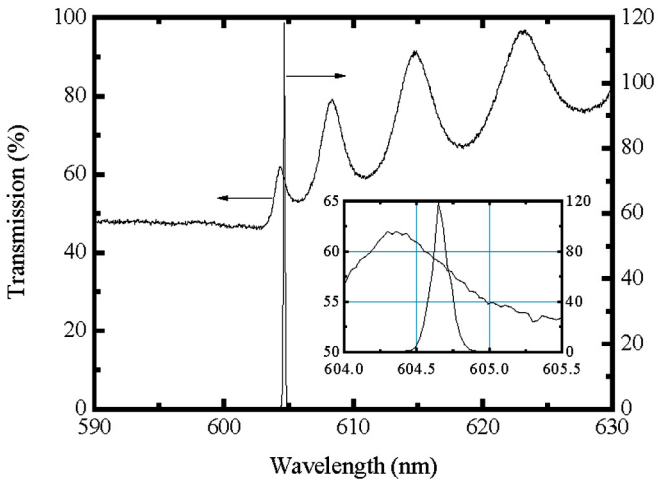

FIGURE 1 — The transmission spectrum for white light showing part of the photonic band-gap and the long-wavelength band-edge (primary y-axis). The laser emission spectrum for a chiral-nematic band-edge laser (secondary y-axis).

ξ_{loc} ~ 4 μm. It was found that to obtain a laser emission spectrum with a narrow linewidth of the order of Δλ = 0.1 nm, the sample had to be prepared so as to exhibit a large monodomain texture. This process, which involves slow cooling the sample and annealing, is discussed in a previous publication.[15]

3.2 Pump spot size

An investigation was carried out to determine the effect the size of the amplifying volume had on the emission characteristics of a liquid-crystal laser.[22] In particular, we were concerned with the change in the excitation threshold and slope efficiency as the pump spot area was varied. The pump spot area was altered by translating the focusing lens along the direction of the pump beam. Figure 2 shows the emission energy as a function of the excitation energy for six different pump spot areas; in each case the laser wavelength is λ = 610 nm. The emission energy from the liquid-crystal sample was collected over a narrow solid angle of 0.12 sr in the forward direction. The figure shows a typical input–output curve that is characteristic of a laser. The solid lines represent the lines of best fit to the data above the excitation threshold.

As the spot size increases, the excitation threshold and slope efficiency are seen to increase and decrease, respectively. For a spot size of d = 90 μm (area = 6.4×10^3 μm^2) the excitation threshold was found to be E_{th} = 3.8 μJ/pulse (fluence ~ 50 mJ/cm^2) whereas for d = 231 μm (area = 42×10^3 μm^2) the excitation threshold was E_{th} = 11.9 μJ/pulse (fluence ~ 17 mJ/cm^2). Therefore, by increasing the spot diameter by a factor of 2.6 (area by a factor of 6.6) the result was a three-fold increase in the excitation threshold energy. It was found that when the threshold energy was plotted as a function of pump area, a linear function best described the relationship. From standard laser physics relating to the

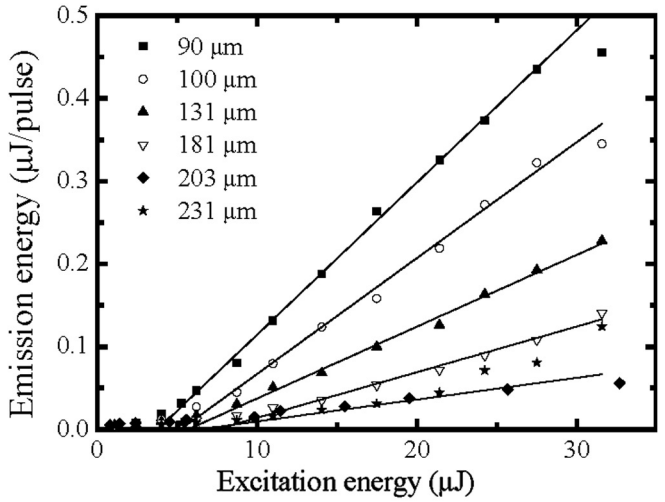

FIGURE 2 — The emission energy as a function of excitation energy of a chiral-nematic band-edge laser for different pump spot diameters.

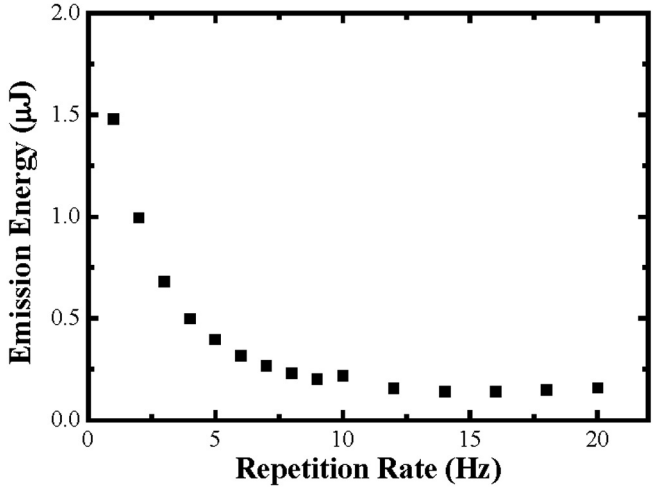

FIGURE 3 — The emission energy of a chiral-nematic band-edge laser as a function of pump repetition rate for an excitation fluence of 450 mJ/cm^2.

space-independent model, the threshold can be shown to be linearly proportional to the cross-sectional pump-beam area, where it is assumed that pump area (mode area) is less than, or equal to, the cross-sectional area of the active medium.[23] On the other hand, for the slope efficiency, this appeared to decrease exponentially with pump spot area.

A somewhat intriguing observation is that the threshold fluence was actually lower for the larger spot size than the smaller spot size. This may be due to the fact that the important factor is actually the cross-sectional area of the laser mode, which is different to the pump area at the sample. Nevertheless, further experimentation is currently being carried out to gain a better understanding of these results.

3.3 Pump repetition rate

An example of the dependence of the emission energy of a chiral nematic band-edge laser on pump repetition rate is shown in Fig. 3: the laser wavelength is λ = 610 nm and the operating temperature is T = 30°C. The plot presents data for 1–20 Hz when the sample is pumped at a fluence of 450 mJ/cm^2. It can be seen that the emission energy decays exponentially with increasing repetition rate; in this case the emission energy at 20 Hz is approximately 10% of that recorded for 1-Hz pulses.

We have considered the possible mechanisms that could be responsible for these observations and there was evidence to suggest that, although there was some bleaching of the dye, there were other mechanistic nonlinear effects that occurred simultaneously during lasing.[24] Specifically, these relate to changes in the director configuration due to either thermal or optical-induced torque effects. Even though it is possible that the local temperature is changing, giving rise to fluctuations in the director, experimental results indicated that the optical field was coupling to the anisotropy of the medium giving rise to an optical torque on the director field. It was found that for an increase in the repetition rate, additional lasers lines appearing at longer wavelengths; the opposite effect to what would be observed if the sample was being heated "locally." Furthermore, it was observed that for the laser dye PM597 in E49*, the helix underwent a pitch jump during the lasing process to a longer pitch. The result was a change in the laser wavelength to longer wavelengths. This would correspond to an optically induced torque effect which would be manifested as a bistability of the helix. For the results presented in this paper all measurements were carried out at 1 Hz.

Of course, the reduction in emission energy for a combination of high excitation energies and high repetition rates poses a significant obstacle with regards to a continuous-wave liquid-crystal laser. At present, we are looking for ways to prevent this behavior from occurring. If it is related to director reorientation due to an optically induced torque effect then polymerization of the structure may help to prevent the helix of the chiral nematic from distorting. On the other hand, if it is due to thermal effects then factors such as the thermal capacity and thermal conductivity of the host need to be considered in more detail.

3.4 Cell thickness

The dependence of the excitation threshold and the slope efficiency on cell thickness is shown in Fig. 4. In this case, the threshold decreases from E_{th} = 12 μJ/pulse at d = 5 μm to E_{th} = 2.5 μJ/pulse between thicknesses of d = 10–15 μm. For each cell thickness the laser line remained at the gain maximum of DCM. Above d = 15 μm, an increase in the thickness results in an increase in the threshold energy. In terms of the slope efficiency, η_s, this is found to increase from η_s = 1.5% at d = 5 μm to η_s ~ 6.5% for thicknesses ranging from d = 10–15 μm. As the cell thickness is increased further, the slope efficiency decreases. The opti-

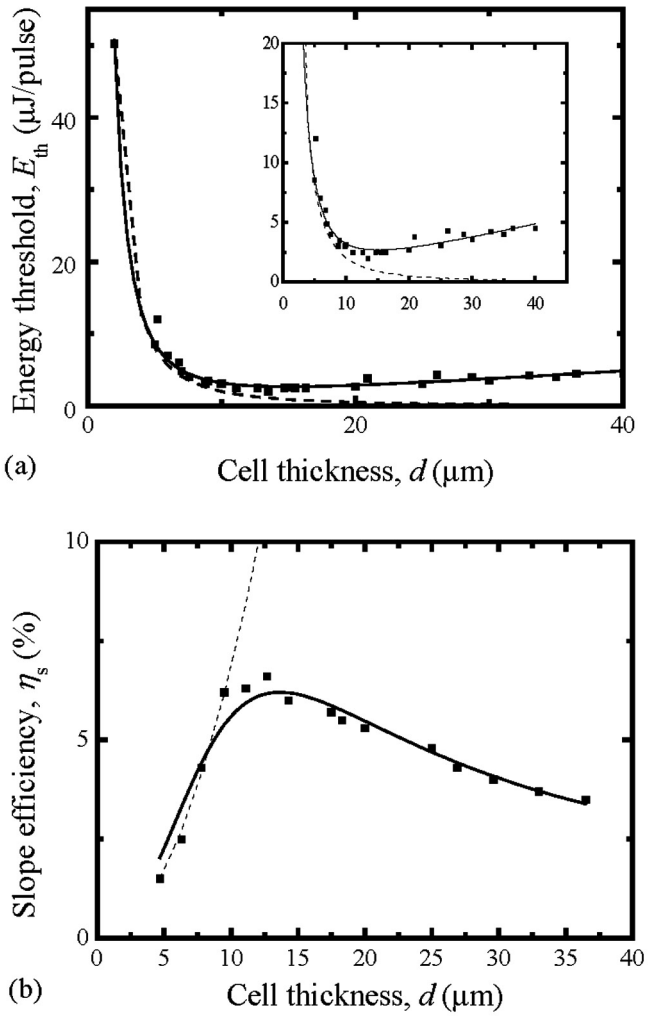

FIGURE 4 — The excitation threshold energy and the slope efficiency as a function of cell thickness for a chiral nematic band-edge laser.

mum value of d, therefore, appears to range between 10 and 15 μm.

A previous report has considered the threshold energy in terms of the threshold gain, γ_{th}.[25] In this case, it was assumed that the threshold energy could be expressed in the form $E_{th} = A(\gamma_{th})d$, where A is a constant and d represents the cell thickness. The parameter A would be related to factors involving the pumping conditions. By considering the threshold gain term in detail it was found that the dependence of the excitation threshold energy on the cell thickness could be expressed as

$$E_{th} = A\left(\alpha + \frac{\beta}{\rho d}\right)d, \tag{1}$$

where α is a coefficient relating to absorption losses, β is a fitting parameter, and ρ is the density of photon states. The authors of Ref. 25 found that $\rho = Bd^2$, where B is a fitting constant specific to the material. This implies that the relationship between the threshold and the cell thickness is of the form $E_{th} \propto d + fn(d^{-2})$. In Fig. 4, the solid line represents the fitting curve using this relationship which is shown to be in good agreement with experimental data.

Alternatively, it is possible to arrive at a similar result by using the same starting point, *i.e.* $[E_{th} = A(\gamma_{th})d]$, but in this case using the threshold gain derived by Kogelnik and Shank for a distributed feedback laser.[26] The threshold energy can then be written as

$$E_{th} = A\alpha d + \frac{A\lambda^2}{\Delta n^2 d^2}, \tag{2}$$

where λ is the wavelength of the laser line and Δn is the birefringence. A recent report has found that the density of states increases as a function of the birefringence which suggests that the material constant B is actually related to the birefringence.[27] Experimentally, we have found that the excitation threshold does appear to change with the birefringence and this is discussed in more detail in the next section.

From both the space-independent and space-dependent rate equations, the slope efficiency can be shown to be proportional to $1/E_{th}$, which in this case would imply that

$$\eta_s \propto \left[d + fn(d^{-2})\right]^{-1}. \tag{3}$$

The solid line in Fig. 4 represents the fitting curve using this expression, and the agreement appears to be rather good. The dashed line in the threshold and slope efficiency graphs represent the condition of no absorption losses, whereby the threshold continues to decrease with increasing thickness to approach a "threshold-less" laser and the slope efficiency increases quadratically with cell thickness.

4 Influence of macroscopic physical properties

Figure 5 shows the threshold and slope efficiency as a function of cell thickness for two liquid-crystal lasers with different birefringence values. In this case, the laser samples are DCM-E49* and DCM-E7* (contains ~3-wt.% BDH1281 and 2-wt.% DCM). The wavelengths of the laser lines are positioned at the gain maximum of DCM (λ = 610 nm). The nematic host E7 (Merck NB-C) is a well-known commercially available nematogen and was chosen as it has a lower birefringence than E49 at T = 30°C (Δn = 0.25, E49 and Δn = 0.20, E7). It can be seen that the DCM-E49* laser exhibits lower laser thresholds than the DCM-E7* laser; although both plots appear to converge at $d \sim 16$ μm.

The solid and dashed curves in Fig. 5(a) represent fitting curves using the relationship

$$E_{th} = P_1 d + \frac{P_2}{d^2}, \tag{4}$$

where $P_1 = A\alpha$ and $P_2 = A\lambda^2/\Delta n^2$. The values for P_1 are found to be the same for both lasers indicating that the absorption losses in both cases were the same. On the other hand,

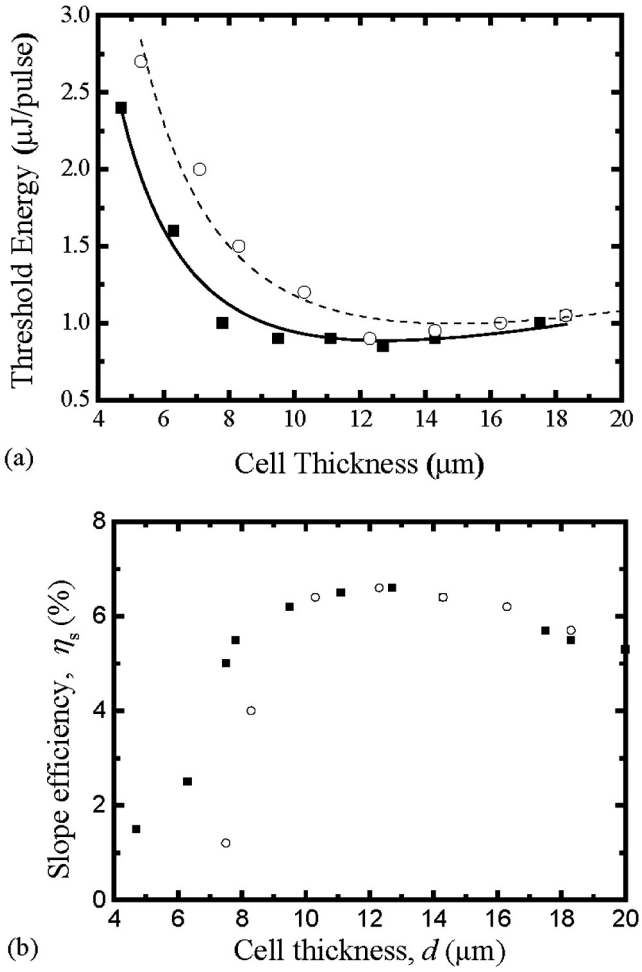

FIGURE 5 — The excitation threshold energy (a) and slope efficiency (b) as a function of cell thickness for DCM-E49* (solid squares) and DCM-E7* (open circles).

the relative values for P_2 are different: for the DCM-E49* and DCM-E7* lasers we obtained $P_2 = 48$ and $P_2 = 73$, respectively. The lower value of P_2 for the DCM-E49* laser does correlate with the higher birefringence of E49 given that $P_2 \propto 1/\Delta n^2$. Furthermore, we recently carried out a similar study[28] with a compound that has a birefringence of $\Delta n = 0.37$ at $T = 30°C$, which is considerably larger than that of E49 and E7, and it was found that the threshold was reduced further corresponding to a smaller value of P_2.

The differences in slope efficiency at thicknesses below $d = 10$ μm are believed to be due to the differences in P_2 which result from the birefringence. We have found that, for a high birefringence liquid crystal, it is actually possible to have a low threshold energy, but at the same time a low slope efficiency.[28] This is because the slope efficiency depends not only on the threshold but also on other factors such as the saturation intensity and additional loss mechanisms. However, in general, we have found that, for a given cell thickness of $d = 7.5$ μm, materials with a high birefringence, high order parameter and large elastic constants tend to have a low threshold and high slope efficiency.[15,29]

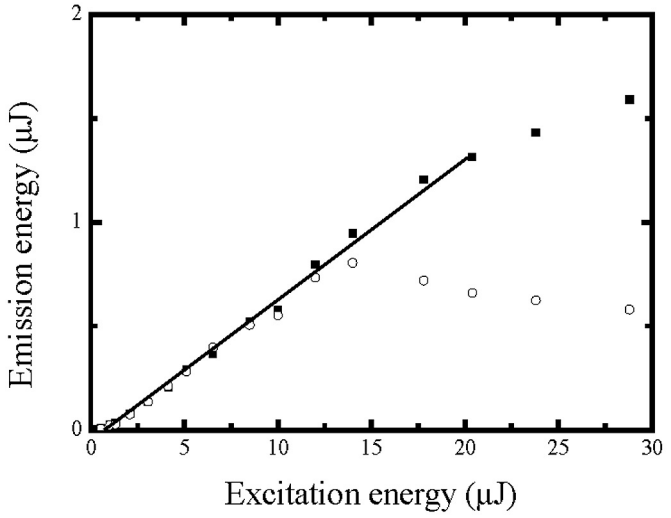

FIGURE 6 — The emission energy as a function of the excitation energy for DCM-E49* (solid squares) and DCM-E7* (open circles) for a fixed cell thickness of $d = 12$ μm.

It is shown in Fig. 5 that the slope efficiency for $d = 12$ μm is the same for both lasers. However, it was found that the saturation emission energy, the energy at which point a further increase in the excitation energy results in a decrease in the emission energy, was lower for DCM-E7* than for DCM-E49*. This is shown in Fig. 6. Often the saturation limit is referred to as the thermal roll-over, although in this case both lasers are operated at the same absolute temperature of $T = 30°C$. It is possible that the thermal capacity or thermal conductivity of DCM-E49* is greater than that of DCM-E7*.

We have found that the performance of a chiral nematic band-edge laser is greatest at the lower temperatures of the chiral nematic mesophase.[30] This is believed to be due to the fact that the macroscopic properties of the liquid-crystal host are maximized at lower temperatures as a result of an increase in the order parameter. However, it should be noted that the performance is not necessarily maximized at lower absolute temperatures. For example, for one laser sample the lowest operating temperature of the chiral nematic mesophase was $T = 95°C$, yet the excitation threshold and slope efficiency were lower and higher than that, respectively, of a laser sample whose lowest operating temperature was $T = 30°C$.

5 Laser dyes

In addition to varying the nematic host, we have also considered the effects of changing the gain medium on the performance of a laser when pumped at $\lambda = 532$ nm. A number of dyes have been examined, including two rhodamine dyes (Lambda Physik) and two pyromethene dyes (Exciton). The emission energy as a function of excitation energy is shown for five different lasers in Figure 7 for pumping at $\lambda = 532$ nm by a Q-switched Nd:YAG laser (NanoT, Litron Lasers) with a repetition rate of 1 Hz. In this instance, the pump

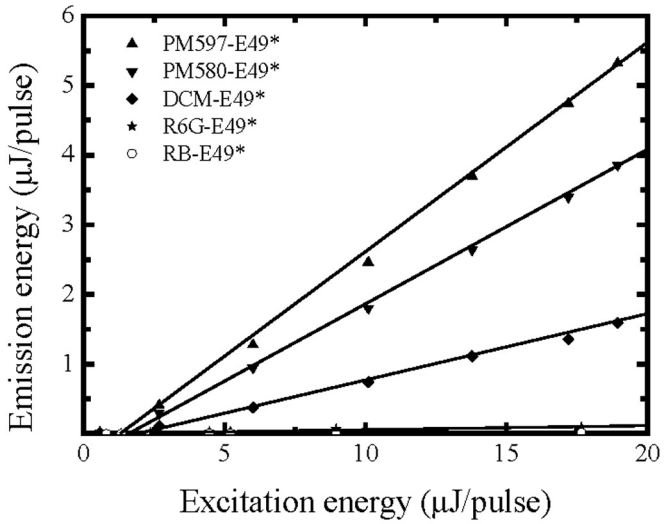

FIGURE 7 — The input-output characteristics for five chiral nematic band-edge lasers with different laser dyes but the same chiral nematic host (E49*). The operating temperature is $T = 31°C$.

spot size and collection solid angle are smaller and larger, respectively, than that used in the previous sections. In all cases, the host is E49 doped with BDH1281: slightly different concentrations of BDH1281 (of the order of 4 wt.%) were required to position the long-wavelength band edge at the gain maximum of each dye. Specifically, the dyes examined were: rhodamine 6G chloride (R6G), rhodamine B chloride (RB), pyrromethene 597 (PM597), pyrromethene 580 (PM580), and DCM. The concentrations by weight of each dye were as follows: 0.3 wt.% for R6G and RB, and 1 wt.% for PM597, PM580, and DCM. The low concentrations of R6G and RB are discussed in more detail below. The laser emission wavelengths are shown in Table 1.

The rhodamine dyes, which are part of the xanthene family, were chosen for two reasons. Firstly, the xanthenes (particularly R6G) are widely used in conventional dye lasers[31] and should therefore provide a useful reference point for the comparison of desirable dye properties for conventional and chiral nematic laser systems. Secondly, the relatively isotropic molecular shape of the rhodamines should prevent guest-host alignment of the dye within the liquid-crystal host,[32] allowing laser-emission characteristics to be interpreted solely in terms of the behavior of each dye in the polar solvent. However, the rhodamines are not readily soluble in liquid-crystal solvents, and it was noted that only a very small percentage (~0.4 wt.%) was required for the dyes to crystallize out of solution.

TABLE 1 — The emission wavelengths of the different chiral-nematic laser samples.

Laser sample	λ (nm)
RB-E49*	582
R6G-E49*	572
PM580-E49*	570
DCM-E49*	609
PM597-E49*	582

Even though these dyes can be considered to be isotropic in terms of molecular shape, the lasing threshold was much lower at the long-wavelength band edge than the short-wavelength edge for both dyes, implying a certain degree of alignment of the transition dipole moment with the liquid-crystal director.[33] For a concentration of 0.3 wt.% dye, the excitation threshold and slope efficiency were found to be lower and higher, respectively, for R6G-E49* than RB-E49*; in this instance, the cell thickness was $d = 14$ μm because it was found that RB-E49* did not generate laser emission in $d = 10$ μm. The slope efficiency of R6G-E49* was found to be $\eta_s = 0.8\%$ as opposed to $\eta_s = 0.1\%$ for RB-E49*. Overall, when doped into E49* both dyes had very low slope efficiencies; this is apparent from Fig. 7 where it can be seen that the outputs are extremely small in comparison to those from the lasers containing 1.0 wt.% of the other three more-elongated dyes (DCM, PM 580, and PM 597) in 10-μm cells. This is due to several factors including weak absorption at the pump wavelength (resulting from the low solubility of the dyes) and poor alignment between the transition dipole moment of the dye and the director. The higher slope efficiency of R6G-E49* is believed to be due to a slightly better alignment of the transition dipole moment of R6G with the director arising from hydrogen bonding between the dye and the liquid-crystal host[34]; these results are discussed in more detail in the literature.[35]

In terms of the input–output characteristics of the other three lasers, DCM-E49*, PM580-E49*, and PM597-E49*, Fig. 7 shows that the emission energies vary rather significantly. The slope efficiencies for each laser are summarized in Table 2, where it can be seen, for example, that η_s for PM597-E49* is a factor of three greater than that of DCM-E49* when excited at $\lambda = 532$ nm and a repetition rate of 1 Hz. The slope efficiency is higher than that presented in the previous sections for DCM-E49* due to the fact that the pump spot size is smaller and the collection solid angle is greater. Of course, the laser wavelength of PM597-E49* is at a shorter wavelength ($\lambda = 582$ nm) than that of DCM-E49* which means that the energy per photon is greater. Taking this into account, we find that the number of photons emitted by the PM597-E49* laser is still a factor of 3 larger (number of photons $\sim 7 \times 10^{12}$) than that of DCM-E49* (number of photons $\sim 2 \times 10^{12}$) when excited with an energy of 10 μJ/pulse. At this stage, it has not yet been determined whether the higher output of PM597-E49* is due to a greater absorption at the excitation wavelength, the quantum efficiency of the dye, or a combination of both factors. Nevertheless, it is noteworthy that the slope efficiency of PM597-E49* is $\eta_s = 29\%$ compared to $\eta_s = 9\%$ for DCM-E49*. The emission energies and slope efficiency of PM580-E49* are between those of the other two lasers. The threshold energies for the three lasers were found to be in the range of $E_{th} \sim 100$–200 nJ/pulse.

TABLE 2 — The slope efficiencies of the different chiral-nematic laser samples.

Laser sample	Slope efficiency, η_s (%)
RB-E49*	0.1
R6G-E49*	0.8
DCM-E49*	9
PM580-E49*	21
PM597-E49*	29

Other dyes have also been considered such as Nile Blue perchlorate and Pyridine 2 perchlorate; however, in both cases the dyes were found to be even less soluble in the liquid-crystal host than the rhodamine dyes. Therefore, for all intents and purposes, they were considered to be insoluble. These dyes, like the rhodamine dyes, are ionic and consequently their solubility in polar liquid-crystal hosts is limited to very small concentrations.

6 3-D photonic band structures

In a recent letter to *Nature*,[36] it was reported that, for certain multi-component mixtures containing bimesogen compounds and a high-twisting-power chiral dopant, blue phase I (BPI) was found to occur naturally over a temperature range of 30°C. The BPI mesophase is a body-centered cubic lattice whereby the spacing of the cubic units is of the order of the wavelength of light. Consequently, this results in a photonic band gap in three-dimensions which means that the blue phase could be used as a three-dimensional band-edge laser by simply adding a gain medium.

In Fig. 8, band-edge lasing from a dye-doped BPI laser is demonstrated. The host mixture was the same as that described in the literature[36] and 1.5 wt.% of DCM was dissolved into the host. The figure shows the laser-emission spectrum for an excitation fluence of 10 mJ/cm^2 at an operating temperature of T = 30°C along with the optical texture that is observed when viewed between the crossed polarizers of an optical polarizing microscope. The platelet from which laser emission occurs is highlighted in the figure and corresponds to the (200) orientation. It can be seen that lasing occurs at λ = 571 nm, corresponding to the band edge of the photonic band gap for the (200) platelet. The band gap of this domain is shifted with respect to the gain maximum of DCM and this is evident from the amplified spontaneous emission (ASE) peak that occurs simultaneously at $\lambda \sim 610$ nm. A number of domains are excited at the same time due to the fact that the sizes of the individual domains are much less than the pump spot size. Due to the wide temperature range of this blue phase, laser emission was observed over a 10°C temperature range with no change in the emission spectrum. The results here show that the laser emission is broader than that of the chiral-nematic laser, although in this case the spectrum was recorded using a 1.3-nm-resolution spectrometer. A recent report[37] has shown that linewidths less than 0.1 nm are achievable indicating a high-quality factor of the laser mode in a single domain of blue phase I.

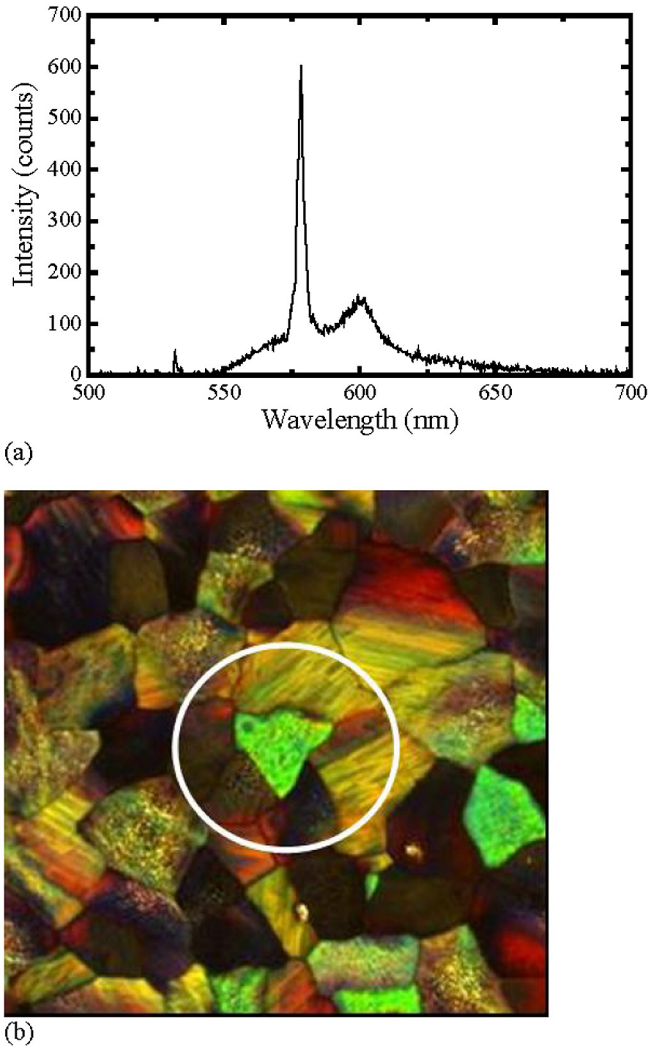

FIGURE 8 — (a) An example of the laser-emission spectrum of a blue-phase I band-edge laser and (b) a micrograph of the optical texture from optical polarizing microscopy between crossed polarizers. The circle in white indicates the platelet from which laser emission occurred.

Achieving laser emission in either BPI or BPII is extremely encouraging as these structures exhibit a photonic band gap in three dimensions unlike the chiral-nematic or chiral-smectic phases. Consequently, both blue phases exhibit a number of important features that are not observed for 1-D photonic band structures. One such feature is that laser emission can occur in multiple directions simultaneously.[19] Ignoring for the time being the technological obstacles that need to be overcome, this could be exploited to produce a single-element red-green-blue light emitter by doping in a number of dyes so as to correspond with the reflection spectrum of the different platelet orientations, *e.g.*, red (110), green (200), and blue (211).

Another very important characteristic is that if the band gap in two of the three-directions is positioned so as to overlap the laser wavelength in the remaining direction, then spontaneous emission into those directions is prohibited. This should result in a further decrease in the threshold. For chiral-nematic and chiral-smectic lasers spontaneous emis-

sion into angles other than the narrow solid angle subtended by the laser mode is a loss mechanism. Control of the lattice spacing in three directions can be achieved, to some extent, with the application of an electric field across the sample. This results in an extension in the lattice spacing in one direction, but a lattice contraction in the other two directions.

Before the advent of the wide-temperature blue phases, either naturally occurring or stabilized with the addition of polymer,[38] it would have been very difficult to envisage the usefulness of blue-phase lasers beyond the academic arena. However, there is still a great deal to be done in terms of understanding why these blue phases exist over such a wide temperature range. Furthermore, procedures for forming a single large-area monodomain texture need to be investigated, although we have already made significant progress in this area and hope to publish the results in the near future.

7 Conclusions

The aim of this paper was to present a review of our recent experimental results regarding the emission characteristics of chiral-nematic band-edge lasers and to consider recent advancements with regards to band-edge lasing from wide-temperature blue phases. In this study we have shown how the performance of a chiral-nematic band-edge laser varies as parameters such as the pump spot size, pump repetition rate, and cell thickness are altered. For large pump spot sizes, the threshold energy is found to be higher than that for small spot sizes, although the fluence at the threshold appears to be lower for larger spot sizes. It was found that for a combination of high excitation energies and high repetition rates, the emission energy is significantly reduced compared to the emission energies obtained for low repetition rates. The dependence of the threshold energy (E_{th}) on cell thickness (d) follows the relationship $E_{th} \propto d + fn(d^{-2})$ in accord with previous observations. In terms of the dependence of the slope efficiency (η_s) on cell thickness, this was found to be best described by considering that $\eta_s \propto 1/E_{th}$. For materials with different values for the birefringence, the fitting parameters were found to be different, whereby a low threshold correlates with a large birefringence. In addition, a number of different laser dyes have been considered and the results show that, for pumping at λ = 532 nm, the laser dye pyrromethene 597 is preferred. Finally, we have demonstrated band-edge lasing in a naturally occurring wide-temperature blue phase I. With such high slope efficiencies, low threshold energies, and narrow linewidths, but with laser outputs tunable throughout the visible spectrum, recent research in this field is beginning to lead to new miniature light sources suitable for novel display applications. Furthermore, the technology is based on well-established liquid-crystalline materials and LCD fabrication techniques, thus simplifying the route to practical applications.

Acknowledgments

The authors would like to gratefully acknowledge the financial support of the EPSRC, UK, and the COMIT Faraday Partnership for CASE studentships with Dow-Corning (ADF) and Merck NB-C (CG). The authors would also like to gratefully acknowledge Dr. Tim Wilkinson for making the wedge cells for the cell-thickness measurements.

References

1 J P Dowling, M Scalora, M J Bloemer, and C M Bowden, *J App Phys* **75**(4), 1896 (1994).
2 V I Kopp, B Fan, H K M Vithana, and A Z Genack, *Opt Lett* **23** (21), 1707 (1998).
3 B Taheri, P Palffy-Muhoray, and H Kabir, ALCOM *Symposium Chiral Materials and Applications* (1999); B Taheri, A Munoz, P Palffy-Muhoray, and R Twieg, *Mol Cryst Liq Cryst* **358**, 73 (2001).
4 M Meier, A Mekis, A Dodabalapur, A Timko, R E Slusher, J D Joannopoulos, and O Nalamasu, *Appl Phys Lett* **74**, 7 (1999).
5 V I Kopp, A Z Genack, and Z-Q Zhang, *Phys Rev Lett* **86** (9), 1753 (2001).
6 A Chanishvili, G Chilaya, G Petriashvili, R Barberi, R Bartolino, G Cipparrone, A Mazzulla, and L Oriol, *Appl Phys Lett* **83**, 5353 (2003).
7 A Y-G Fuh, T-H Lin, J-H Liu, and F-C Wu, *Opt Exp* **12**, 1857 (2004).
8 A Chanishvili, G Chilaya, G Petriashvili, R Barberi, R Bartolino, G Cipparrone, A Mazzulla, and L Oriol, *Adv Mater* **16**, 791 (2003).
9 S Furumi, S Yokoyama, A Otomo, and S Mashiko, *Appl Phys Lett* **84**, 2491 (2004).
10 K Funamoto, M Ozaki, and K Yoshino, *Jpn J Appl Phys* **42**, 1523 (2003).
11 J R Willmott, S M Morris, A E Blatch, M J Coles, and H J Coles, Oral presentation at *International Liquid Crystals Conference*, **C65** (2002).
12 H Finkelmann, S T Kim, A Munoz, P Palffy-Muhoray, and B Taheri, *Adv Mater* **12**, 1069 (2001).
13 M Ozaki, M Kasano, D Ganzke, W Haase, and K Yoshino, *Adv Mater* **14**, 306 (2002).
14 S Furumi, S Yokoyama, A Otomo, and S Mashiko, *Appl Phys Lett* **82**, 16 (2003).
15 S M Morris, A D Ford, B J Broughton, M N Pivnenko, and H J Coles, *P Soc Photo-Opt Ins* **5741**, 118 (2005).
16 M Ozaki, M Kasano, D Ganzke, W Hasse, and K Yoshino, *Adv Mater* **14**, 306 (2002).
17 A D Ford, S M Morris, M N Pivnenko, and H J Coles, *P Soc Photo-Opt Ins* **5289**, 213 (2004).
18 S Yokoyama, S Mashiko, H Kikuchi, K Uchida, and T Nagamura, *Adv Mater* **18**, 48 (2006).
19 W Cao, A Munoz, P Palffy-Muhoray, and B Taheri, *Nature Mater* **1**, 111 (2002).
20 S John and T Quang, *Phys Rev Lett* **74**, 3419 (2005).
21 Y Zhou, Y Huang, A Rapaport, M Bass, S–T Wu, *Appl Phys Lett* **87**, 231107 (2005).
22 S M Morris, A D Ford, M N Pivnenko, and H J Coles, *Appl Phys Lett* (submitted).
23 O Svelto, *Principles of Lasers*, 4th ed. (Plenum Press, New York, 1998).
24 S M Morris, A D Ford, M N Pivnenko, and H J Coles, *J Opt A: Pure Appl Opt* **7**, 215 (2005).
25 W Cao, P Palffy-Muhoray, B Taheri, A Marino, and G Abbate, *Mol Cryst Liq Cryst* **429**, 101 (2005).
26 H Kogelnik and C V Shank, *J Appl Phys* **43**, 2327 (1972).
27 K L Woon, M O'Neill, G J Richards, M P Aldred, and S M Kelly, *Phys Rev E* **71**, 041706 (2005).
28 A D Ford, S M Morris, M N Pivnenko, S Gauza, S–T Wu, and H J Coles, *Liq Cryst* (submitted).
29 A D Ford, S M Morris, M N Pivnenko, and H J Coles, *P Soc Photo-Opt Ins* **5741**, 217 (2005).
30 S M Morris, A D Ford, M N Pivnenko, and H J Coles, *J Appl Phys* **97**, 023103 (2005).
31 T G Pavlopoulos, *Prog Quant Elect* **26**, 193 (2002).
32 H V Ivashchenko and V G Rumyantsev, *Mol Cryst Liq Cryst* **150A** (1987).
33 J Schmidtke and W Stille, *Euro Phys B* **31**, 179 (2003).

34 L Marrucci, D Paparo, M R Vetrano, M Colicchio, E Santamato, and G Viscardi, *J Chem Phys* **113**, 10361 (2000).
35 C Gillespie, S M Morris, and H J Coles, *P Soc Photo-Opt Ins* **5741**, 135 (2005).
36 H J Coles and M N Pivnenko, *Nature* **436**, 998 (2005).
37 S Yokoyama, S Mashiko, H Kikuchi, K Uchida, and T Nagamura, *Adv Mater* **18**, 48 (2006).
38 H Kikuchi, M Yokota, Y Hisakado, H Yang, and T Kajiyama, *Nature Mater* **1**, 64 (2002).

Stephen Morris obtained his M.S. degree in physics from the University of Southampton in 2000. Under the supervision of Professor Harry Coles he is currently finishing his Ph.D. in liquid crystals for linear and nonlinear photonics applications, at the Centre of Molecular Materials for Photonics and Electronics, Cambridge University Engineering Department. His research interests include the flexoelectro-optic effect, liquid-crystal lasers, and polymer-dispersed liquid crystals. He was sponsored by both Merck NB-C and the Engineering and Physical Sciences Research Council.

Alison Ford received her M.S. degree in physics from the University of Southampton in 2001. Since 2002, she has been studying the emission properties of liquid-crystal lasers during her Ph.D. program at the Centre of Molecular Materials for Photonics and Electronics of the electrical engineering department at the University of Cambridge. She was sponsored by both Merck NB-C and the Engineering and Physical Sciences Research Council.

Carrie Gillespie graduated from Heriot-Watt University in 2002 with an M.S. degree in physics of optoelectronics and laser engineering. Since 2002, she has been a Ph.D. student at the Centre of Molecular Materials for Photonics and Electronics at the University of Cambridge, where she is also a member of Wolfson College. Her research is concerned with lasing dye-doped chiral-nematic liquid crystals and their use in photonic devices. This work is conducted in association with her CASE sponsor, Merck NB-C and the Engineering and Physical Sciences Research Council.

Mikhail Pivnenko received his M.Sc. degree in engineering from Kharkov University (Ukraine) in 1986. Between 1986 and 1996, he was involved in theoretical research on electrodynamics of condensed media. After completing his doctoral studies on the physics of liquid crystals in 2001, he joined the Liquid Crystal Group at the University of Southampton. He is now a Research Fellow at the Centre of Molecular Materials for Photonics and Electronics at Cambridge University Engineering Department. His research interests include wide-temperature-range blue phases, liquid-crystal lasers, and ferroelectric liquid crystals.

Oliver Hadeler received his diploma in physics from the University of Frankfurt, Germany in 1995, and his Ph.D. in optoelectronics, from the University of Southampton, England in 2002. During his time at the Optoelectronics Research Centre in Southampton, he carried out both theoretical and experimental work on distributed feedback fiber lasers for telecommunication and sensor applications. In 2001, he joined the Liquid Crystal Group in the Physics Department at Southampton University where he investigated liquid-crystal devices for telecommunication applications. Since 2002, he is with the Engineering Department at the University of Cambridge, U.K., where his areas of research are liquid-crystal telecommunication devices, displays, and liquid-crystal lasers.

Harry Coles is Professor of photonics of molecular materials at the Engineering Department of Cambridge University and Director of the multidisciplinary Cambridge Centre of Molecular Materials for Photonics and Electronics and Fellow of the Institute of Physics. His research interests cover extremely wide areas: synthesis and characterization of liquid crystals, oligomers, and polymers; structure-property correlations; spectroscopic and electro-optic techniques; linear and non-linear optics of liquid crystals; organic lasers; thin-film optical devices; and displays; telecommunications and photonic switches/interconnects, device fabrication. To date, he has published over 200 refereed papers, 24 patents, and some 400 published abstracts. He is also Managing Director of COMIT, a Faraday Partnership devoted to **Co**mmunications and **M**obile **I**nformation **T**echnology involving the Universities of Bristol, Cambridge, Exeter, Hull, Oxford, and NTU and over 20 Companies. In 2002, he was invited by the British Liquid Crystal Society to give the Ben Sturgeon Memorial Lecture and in April 2003 was awarded the George Gray Medal for his research on Liquid Crystals and their Applications. He was recently elected Professorial Fellow of St Catharine's College, University of Cambridge.